Available online at www.sciencedirect.com

SciVerse ScienceDirect

journal homepage: www.elsevier.com/locate/watres

Facilitated transport of Cu with hydroxyapatite nanoparticles in saturated sand: Effects of solution ionic strength and composition

Dengjun Wang [a,g], *Marcos Paradelo* [b], *Scott A. Bradford* [c], *Willie J.G.M. Peijnenburg* [d,e], *Lingyang Chu* [a,f], *Dongmei Zhou* [a,*]

[a] *Key Laboratory of Soil Environment and Pollution Remediation, Institute of Soil Science, Chinese Academy of Sciences, Nanjing 210008, PR China*

[b] *Soil Science Group, Department of Plant Biology and Soil Science, Faculty of Sciences, University of Vigo, Ourense E-32004, Spain*

[c] *US Salinity Laboratory, Agricultural Research Service, United States Department of Agriculture, 450 W. Big Springs Road, Riverside, CA 92507, USA*

[d] *Laboratory of Ecological Risk Assessment, National Institute of Public Health and the Environment, P.O. Box 1, 3720 BA Bilthoven, The Netherlands*

[e] *Institute of Environmental Sciences (CML), Leiden University, P.O. Box 9518, 2300 RA Leiden, The Netherlands*

[f] *College of Resources and Environmental Sciences, Anhui Agricultural University, Hefei, 230036, PR China*

[g] *Graduate School of the Chinese Academy of Sciences, Beijing 100049, PR China*

ARTICLE INFO

Article history:
Received 2 May 2011
Received in revised form
23 August 2011
Accepted 24 August 2011
Available online 16 September 2011

Keywords:
Hydroxyapatite nanoparticles (nHAP)
Cu
nHAP-facilitated Cu (nHAP-F Cu)
Co-transport
Ionic strength (IS)
Ionic composition (IC)

ABSTRACT

Column experiments were conducted to investigate the facilitated transport of Cu in association with hydroxyapatite nanoparticles (nHAP) in water-saturated quartz sand at different solution concentrations of NaCl (0–100 mM) or $CaCl_2$ (0.1–1.0 mM). The experimental breakthrough curves and retention profiles of nHAP were well described using a mathematical model that accounted for two kinetic retention sites. The retention coefficients for both sites increased with the ionic strength (IS) of a particular salt. However, the amount of nHAP retention was more sensitive to increases in the concentration of divalent Ca^{2+} than monovalent Na^{+}. The effluent concentration of Cu that was associated with nHAP decreased significantly from 2.62 to 0.17 mg L^{-1} when NaCl increased from 0 to 100 mM, and from 1.58 to 0.16 mg L^{-1} when $CaCl_2$ increased from 0.1 to 1.0 mM. These trends were due to enhanced retention of nHAP with changes in IS and ionic composition (IC) due to compression of the double layer thickness and reduction of the magnitude of the zeta potentials. Results indicate that the IS and IC had a strong influence on the co-transport behavior of contaminants with nHAP nanoparticles.

1. Introduction

Nanotechnology focuses on the investigation and application of materials with at least one characteristic dimension less than 100 nm. Properties of nanomaterials such as small size, high surface area per unit volume and great reactivity make them a highly promising class of materials for a variety of potential applications. For example, hydroxyapatite nanoparticles

* *Corresponding author*. Tel./fax: +86 25 86881180.
E-mail address: dmzhou@issas.ac.cn (D. Zhou).

0043-1354/$ – see front matter © 2011 Elsevier Ltd. All rights reserved.
doi:10.1016/j.watres.2011.08.041

($Ca_{10}(PO_4)_6(OH)_2$, nHAP), which are the main component of hard tissues of vertebrates such as bones and teeth, have been widely applied for the remediation of contaminated soil and purification of wastewaters polluted by metal ions and actinides (Cu^{2+}, Pb^{2+}, Cd^{2+}, Co^{2+}, and Sr^{2+}) because of their strong ability to fix them (Ma et al., 1994; Smiciklas et al., 2006; Handley-Sidhu et al., 2011). The fixation of metal ions on nHAP may take place through one or more mechanisms, including: ion exchange, surface complexation, and dissolution of nHAP to form new metal phosphates (Ma et al., 1994; Smiciklas et al., 2006; Handley-Sidhu et al., 2011).

To date, little attention has been paid to potential environmental risks of using nHAP to remediate soils contaminated by heavy metals. Specifically, nHAP may alter the transport and fate of common environmental metal contaminants, such as Cu, by dramatically affecting their distribution among mobile and immobile phases (Wang et al., 2011). The transport potential of many chemicals is known to be greatly enhanced when they are associated with mobile colloids (McCarthy and Zachara, 1989; de Jonge et al., 2004; Simunek et al., 2006; Bradford and Kim, 2010). This process is often referred to as "colloid-facilitated contaminant transport" (Grolimund et al., 1996; Roy and Dzombak, 1997). Colloid-facilitated contaminant transport in subsurface environments has attracted considerable attention in recent years, especially for nanoscale colloids such as buckminsterfullerene (Zhang et al., 2011) and TiO_2 (Fang et al., 2011). However, essentially no published data are available on how nHAP might mediate the transport and fate of Cu in subsurface environments.

The solution ionic strength (IS) and composition (IC) are known to have a large influence on the transport behavior of colloid-associated contaminants. For example, Cheng and Saiers (2010) reported that the capacity of sediment-colloids to bind ^{137}Cs decreased with increasing IS (Na^+ cation), leading to a decrease of the mass of ^{137}Cs eluted from columns packed with Hanford coarse sand. Walshe et al. (2010) found that increasing the IS (Ca^{2+} cation) of the bulk solution reduced peak concentrations for both kaolinite and kaolinite-facilitated MS2 coliphage from columns composed of gravel aquifer media. The influence of IS and IC on colloid and nanoparticles interactions with solid surfaces is typically explained using theory developed by Derjaguin–Landau–Verwey–Overbeek (Derjaguin and Landau, 1941; Verwey and Overbeek, 1948). This theory predicts that increasing the solution IS tends to decrease the double layer thickness and magnitude of the surface charge, and thereby increase colloid retention. Divalent ions have a greater effect on these properties than monovalent ions (Israelachvili, 1992; Elimelech et al., 1995). However, up till now there has been no systemic investigation concerning the effects of IS on the co-transport behavior of Cu with nHAP. Furthermore, divalent Ca^{2+} can compete with Cu for ion-exchange sites of nHAP, leading to enhance dissociation of Cu^{2+} from nHAP, and thus altering the co-transport behavior of Cu with nHAP. It is therefore crucial to investigate the impact of the divalent Ca^{2+} on the co-transport behavior of Cu with nHAP in saturated packed columns. The overall objective of this study was to systemically investigate the effects of solution IS and IC on the co-transport of Cu with nHAP.

2. Materials and methods

2.1. Quartz sand

Quartz sand (Sinopharm Chemical Reagent Co., Ltd., China) was used as column packing material. The grain size distribution of the sand was determined by sieve analysis. The median grain size (d_{50}) of the sand was 600 μm, and the coefficient of uniformity ($U_i = d_{60}/d_{10}$ where x% of the mass was finer than d_x) was 1.3. Prior to use, the sand was cleaned thoroughly by the procedure described elsewhere (Zhou et al., 2011) to remove any metal oxide and absorbed clay on the sand surface. The ζ-potential of the quartz colloid was measured by the method described in our previous work (Wang et al., 2011; Zhou et al., 2011).

2.2. nHAP

The nHAP used in this study (purity >99.9%) was purchased from Aipurui Nanomaterial Company (Nanjing, China). The physicochemical properties of the nHAP were determined in our previous work (Wang et al., 2011). Briefly, the nHAP particles are rod-shaped and their mean size is 20 nm in width and 100 nm in length, the Ca/P molar ratio is 1.65 and the specific surface area of the nHAP is 154 $m^2\ g^{-1}$.

2.3. Co-transport tests

Cleaned quartz sand was dry-packed into a glass chromatographic column (20 cm × 2.6 cm, Shanghai, China) with 80 μm stainless-steel screens on both ends. Each column contained approximately 150 g of quartz sand and had an average length of 20 cm. To achieve uniform packing, the sand was carefully added to the column using a spatula and then gently vibrated. The column was slowly saturated by pumping ultrapure water (18.2 MΩ, Millipore, Inc., USA) in the upward direction at an approach velocity of 0.1 cm min^{-1} for 1 h. Following this saturated step, the water content of each column was determined gravimetrically. The porosity of the packed columns varied between 0.39 and 0.41. Table 1 shows the most salient properties of the packed columns used in the co-transport tests of nHAP. The longitudinal dispersivity of the packed column was estimated from transport tests using bromide as tracer.

Table 1 – Properties and parameters of the nHAP and packed quartz sand columns used in this study.

nHAP length (L) nm	100
nHAP width (L) nm	20
nHAP density (ρ_n) g cm^{-3}	3.2
Collector diameter (d_c) mm	0.6
Fluid density (ρ_f) kg m^{-3}	10^3
Fluid viscosity (μ) kg m^{-1} s^{-1}	8.9×10^{-4}
Temperature (T) K	293
Hamaker constant (A) J	1.0×10^{-20}
Porosity (f) cm^3 cm^{-3}	0.39–0.41
Column length (L) cm	20.0
Column diameter (L) cm	2.6
Happel model parameter (A_s)	36.1–41.2

To determine the effects of IS and IC on the co-transport behavior of Cu with nHAP, Cu-bearing nHAP suspensions at varying ISs and ICs were prepared as follows. First, 0.10 g of nHAP powder and 50 mL ultrapure water were added to a 500 mL volumetric flask and shaken vigorously for 1 min to disperse the nHAP. Then, 50 mL of 1.0 mM $Cu(NO_3)_2$ (analytical grade) and 400 mL of different concentrations of NaCl or $CaCl_2$ solution were added. The final volume was 500 mL, and the concentrations of nHAP and Cu in suspension were 200 mg L^{-1} and 0.1 mM, respectively. The electrolyte concentrations added to the suspension were 0, 1, 10, 50, and 100 mM of NaCl or 0.1, 0.3, 0.5, and 1.0 mM of $CaCl_2$. The nHAP suspensions were sonicated for 30 min before use. The ζ-potentials of the Cu-bearing nHAP suspensions were measured using a micro-electrophoresis instrument (JS94 G, Zhongcheng Digital Technology Co., Ltd., Shanghai, China).

2.4. Experimental design

Packed columns were initially equilibrated by flushing several pore volumes (PVs) of ultrapure water and at least 5 PVs of the colloid-free background electrolyte solution in order to establish steady state flow and to standardize the chemical conditions. Experiments was conducted in the following steps: (1) phase 1, the Cu-bearing nHAP suspensions in solutions of varying IS and IC (as described in Section 2.3) were gently stirred while applied to the bottom end of the column *via* a peristaltic pump (YZΠ-15, Baoding Longer Precision Pump Co., Ltd., Hebei, China) at a constant approach velocity (0.44 cm min^{-1}) for about 3.75 PVs, and (2) phase 2, several PVs of nHAP-free background electrolyte solution with the same pH and IS were pumped into the column to ensure that almost no colloidal particles were detected in the effluent. Column outflow was collected in 15-mL glass tubes at regular time intervals using a fraction collector (BS-100A, Huxi Analytical Instrument Factory Co., Ltd., Shanghai, China). All column experiments were conducted in duplicate.

Following the completion of each co-transport test, the spatial distribution of nHAP retained in the column was determined. The fitting at the column end was removed, and the quartz sands were carefully excavated in 2 cm increments and transferred into ten 50 mL vials. Excess ultrapure water was added to fill the vials. In this low IS solution, highly negatively charged surfaces of both nHAP and quartz sand grains caused the release of retained nHAP from the sand surface. After 1 h, the vials containing the sand-nHAP solution were gently shaken to obtain a homogeneous concentration of nHAP in the supernatant. The concentration of nHAP in the excess aqueous solution was measured with a UV/vis spectrophotometer (see Section 2.5.1). The sand samples were then oven dried at 100 °C overnight to obtain the dry weight of the solid. A mass balance was calculated for nHAP in the effluent and retained in the sand after normalizing by the total amount of nHAP injected into the column.

After completion of the co-transport experiment with 1.0 mM of $CaCl_2$, some of the quartz sand grains that were excavated from the inlet of the packed column were examined using a SEM-EDX (Scanning Electron Microscope-Energy Dispersive X-ray, SSX-550, Shimadzu) to determine mechanisms of nHAP retention in the sand columns.

2.5. Analytical procedures

2.5.1. Concentration of nHAP and Cu in the effluent

The concentrations of nHAP in the outflow were determined with a UV/vis spectrophotometer (721-100, Jinghua Science and Technology Instrument Co., Ltd., Shanghai, China), at a wavelength of 300 nm (Wang et al., 2011). A calibration curve was constructed by diluting a 200 mg L^{-1} suspension of nHAP. Spectrometer response versus nHAP concentration was linear in the range of 0–200 mg L^{-1} with a coefficient of determination of $R^2 = 0.999$. The calculated molar extinction coefficient of nHAP was 4.0×10^3 M^{-1} cm^{-1} which was consistent with the result observed by Boussiba and Richmond (1979). The detection lower limit was 1.0 mg L^{-1}. The calibration curve was verified to be independent of the solution chemistry for our experimental conditions.

Aliquots (5 mL) of all effluents were centrifuged at 170,000× *g* for 1 h (Optima TM L-80XP Ultracentrifuge, Beckman) and then filtered through a 0.22 μm membrane filter to determine the dissolved Cu. Five mL of 16 M HNO_3 was added to other aliquots (5 mL) of all effluents to determine the total Cu concentration. The nHAP-facilitated (nHAP-F) Cu was calculated as the difference between total and dissolved Cu. The Cu concentration was determined using an Atomic Absorption Spectrophotometer (AAS, Hitachi Z-2000, Japan).

2.5.2. Size of Cu-bearing nHAP colloid

The average Cu-bearing nHAP aggregate size and the intrinsic size distributions in various suspensions were measured using dynamic light scattering (DLS) (BI-200 SM, Brookhaven Instrument Corp., USA) at 25 °C. The CONTIN algorithm was used to convert intensity autocorrelation functions to an intensity-weighted, Cu-bearing nHAP aggregate, hydrodynamic diameter distribution based on the Stokes–Einstein equation (Stankovich et al., 2006). The intensity-weighted distributions were further converted to number-weighted size distribution, using 1.56 as the refractive index for nHAP (Onuma et al., 2000).

2.5.3. Data analysis

The transport of nHAP through the packed columns was described using a one-dimensional form of the convection–dispersion equation with two kinetic retention sites as (Schijven and Simunek, 2002; Bradford et al., 2003):

$$\frac{\partial \theta c}{\partial t} + \rho_b \frac{\partial (s_1)}{\partial t} + \rho_b \frac{\partial (s_2)}{\partial t} = \frac{\partial}{\partial x}\left(\theta D \frac{\partial c}{\partial x}\right) - \frac{\partial qc}{\partial x} \quad (1)$$

where θ is the volumetric water content [−], c is the Cu-bearing nHAP colloid concentration in the aqueous phase [N L^{-3}, where N and L denote number and length, respectively], ρ_b is the bulk density of the porous matrix [M L^{-3}, where M denotes mass], t is the time [T], x is the vertical spatial coordinate [L], D is the hydrodynamic dispersion coefficient [L^2 T^{-1}], q is the flow rate [L T^{-1}], and s_1 [N M^{-1}] and s_2 [N M^{-1}] are the solid phase concentrations associated with retention sites 1 and 2, respectively.

The two kinetic retention sites described mass transfer of nHAP between the aqueous and solid phase. The first kinetic

site (site 1, Eq. (2)) assumes reversible retention, whereas the second kinetic site (site 2, Eq. (3)) assumes irreversible, depth-dependent retention as:

$$\rho_b \frac{\partial(s_1)}{\partial t} = \theta k_1 c - \rho_b k_{1d} s_1 \quad (2)$$

$$\rho_b \frac{\partial(s_2)}{\partial t} = \theta k_2 \psi_x c \quad (3)$$

where k_1 [T^{-1}] and k_2 [T^{-1}] are first-order retention coefficients on site 1 and 2, respectively, k_{1d} [T^{-1}] is the first-order detachment coefficient, and ψ_x [–] is a dimensionless function to account for depth-dependent retention. The value of ψ_x is given as (Bradford et al., 2003):

$$\psi_x = \left(\frac{d_c + x - x_0}{d_c}\right)^{-\beta} \quad (4)$$

where d_c is the median diameter of the sand grains [L], x_0 is the coordinate [L] of the location where the depth-dependent retention starts and β is an empirical factor controlling the shape of the spatial distribution. Bradford et al. (2003) found that a value of 0.432 provides an optimum for experiments in which significant depth-dependency occurred. The above approach assumes that retention near the column inlet is dominated by site 2, and away from the inlet by site 1.

It should be mentioned that some researchers have attributed attachment/detachment and straining mechanisms of colloid retention to sites 1 and 2, respectively (e.g., Bradford et al., 2003; Gargiulo et al., 2007, 2008). However, additional microscopic information is frequently needed to substantiate this assumption. In this work we do not attempt to attribute specific nHAP retention mechanisms to a given site without other experimental evidence. Rather, Eqs. (1)–(4) are viewed as a simple and flexible approach to describe nHAP breakthrough curves and retention profiles that are not exponential with depth.

Breakthrough curves (BTCs) and retention profiles, obtained from the experiments above, were analyzed using the HYDRUS-1D code (Simunek et al., 2008), which allowed us to fit the nHAP transport parameters (k_1, k_{1d}, and k_2) using a nonlinear least square optimization routine based on the Levenberg–Marquardt algorithm (Marquardt, 1963). The approach velocity and dispersivity that were used in the Hydrus-1D code were obtained by fitting the solution of the convective dispersion equation for the tracer (bromide) breakthrough curves.

3. Results and discussion

3.1. Properties of Cu-bearing nHAP and collector surface

Electrokinetic potential (ζ-potential) will affect the retention and transport behavior of Cu-bearing nHAP. The measured ζ-potentials of the Cu-bearing nHAP and quartz sand (colloidal fragments) in solutions of varying IS and IC became less negative as the electrolyte concentration of the bulk solution increased (Table 2). This is due to the compression of the electrostatic double layer (Elimelech et al., 1995). With the monovalent Na^+ as the background electrolyte, the ζ-potential of Cu-bearing nHAP and quartz colloids decreased from −79.6 to −24.7 mV and from −51.2 to −20.0 mV, respectively, when the IS was increased from 0 to 100 mM. In the case of the divalent Ca^{2+}, the ζ-potential of Cu-bearing nHAP declined from −34.9 to −22.1 mV when the Ca^{2+} concentration in the bulk solution was increased from 0.10 to 1.0 mM. It is obvious that the divalent Ca^{2+} is significantly more effective at screening the surface charge of nHAP than the monovalent Na^+. Similar results have been observed elsewhere (Kim et al., 2010; Wang et al., 2011).

Table 2 presents the average hydrodynamic sizes of 200 mg L^{-1} Cu-bearing nHAP suspensions in the various IS and

Table 2 – Properties of Cu-bearing nHAP suspensions at varying ISs and ICs used in transport tests.

NaCl (mM)	$CaCl_2$ (mM)	pH	Size[a] (nm)	ζ-potential (mV)		Φ_{max}[c] (kT)	Φ_{min2}[d] (kT)	h[e] (nm)	Total Cu[f] (mg L^{-1})	Dissolved Cu[g] (mg L^{-1})
				Quartz sand	nHAP colloid[b]					
0	0	5.7	100 ± 2	−79.6 ± 1.2	−53.0 ± 2.8	NA[h]	NA	NA	6.65	2.42
1.0	0	5.8	102 ± 3	−71.0 ± 1.0	−35.2 ± 0.7	160	−1.6	48	6.56	2.44
10	0	5.9	108 ± 5	−50.2 ± 0.8	−31.4 ± 0.8	121	−4.1	16	6.56	2.43
50	0	5.8	119 ± 4	−35.8 ± 0.9	−25.8 ± 1.2	82	−7.7	7	6.65	2.46
100	0	5.8	133 ± 4	−24.7 ± 1.2	−20.0 ± 1.3	44	−11	4	6.60	2.45
0	0.10	5.9	103 ± 4	−47.0 ± 1.4	−34.9 ± 1.2	138	−1.3	58	6.61	2.38
0	0.30	5.8	109 ± 5	−36.2 ± 0.7	−31.5 ± 0.9	108	−2.1	37	6.65	2.57
0	0.50	5.7	114 ± 3	−31.7 ± 0.9	−28.4 ± 0.5	54	−2.7	28	6.62	2.73
0	1.0	5.7	135 ± 5	−26.0 ± 1.1	−22.1 ± 1.2	48	−4.4	19	6.59	2.96

a The average particle hydrodynamic size, determined by DLS measurement.
b ζ-potential of the Cu-bearing nHAP colloid.
c The maximum energy barrier, Φ_{max}, calculated by DLVO theory.
d The secondary minimum, Φ_{min2}, calculated by DLVO theory.
e Separation distance from colloid surface to secondary minimum.
f Total Cu concentration of the Cu-bearing nHAP suspension.
g Dissolved Cu concentration in the bulk solution.
h Not applicable.

IC solutions. The nHAP size increased from 100 to 133 nm as the concentration of NaCl increased from 0 to 100 mM, and from 103 to 135 nm as the concentration of $CaCl_2$ increased from 0.1 to 1.0 mM of $CaCl_2$. Similar results have been observed by Chen and Elimelech (2006, 2007). These nHAP sizes were used for the interaction energy calculations between nHAP and quartz sand provided in Table 2. Both Cu-bearing nHAP and quartz were negatively charged for all the considered IS and IC. Consequently, electrostatic repulsion occurred between Cu-bearing nHAP and quartz (energy barrier ranged from 44 to 160), even for the highest electrolyte concentration used in the column transport experiments. However, the theoretical prediction of the DLVO interaction energy for nHAP upon their approach to the collector surface shows the presence of a secondary minimum (Table 2) that ranged from −1.3 to −11 depending on the IS and IC. The height of the primary energy barrier decreases and the depth of the secondary minimum increases with IS. This behavior is due to compression of the diffuse double layer thickness with increasing IS according to standard Poisson–Boltzmann theory. Therefore, nHAP are likely to interact with the quartz surface in the secondary minimum, especially at higher IS.

3.2. Co-transport behavior of Cu-bearing nHAP

Results of Cu-bearing nHAP transport studies with various concentrations of NaCl (0, 1, 10, 50, and 100 mM) and $CaCl_2$ (0.1, 0.3, 0.5, and 1.0 mM) are shown in Figs. 1 and 2, respectively. Breakthrough curves are plotted in Figs. 1 and 2a as the relative effluent concentration (C_i/C_0, where C_i and C_0 are the effluent and influent concentration of Cu-bearing nHAP, respectively) as a function of PVs. Retention profiles are plotted in Figs. 1 and 2b as normalized concentration (quantity of the Cu-bearing nHAP recovered in the sand, N_t, divided by the quantity in a unit volume of the input nHAP suspension, N_0) per gram of dry sand as a function of distance from the column inlet. The corresponding mass recovery of nHAP in the effluent and sand is shown in Table 3. Very good total mass balance was obtained for nHAP and Cu (90–96% and 87–95%, respectively), which provides a high degree of

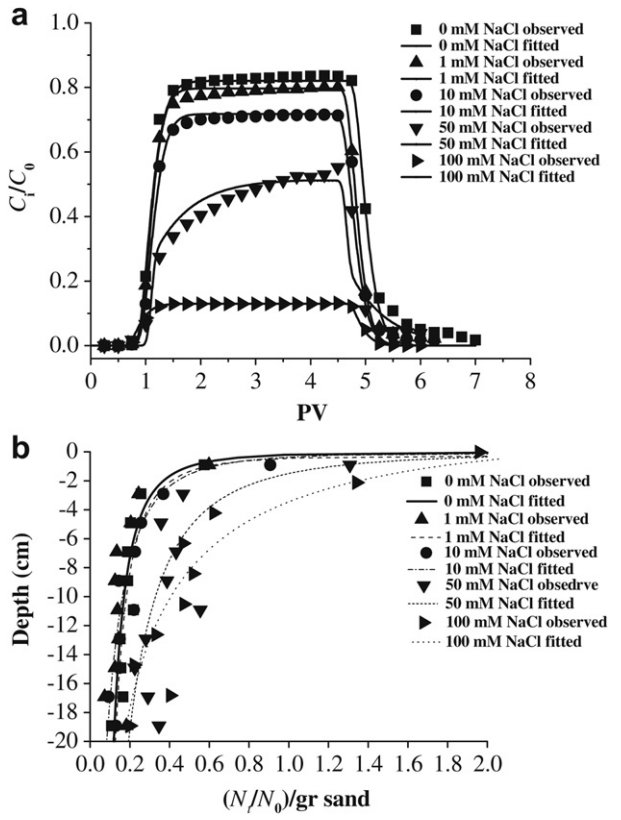

Fig. 1 – Measured and fitted breakthrough curves (a) and retention profiles (b) for nHAP under the IS of 0, 1, 10, 50 and 100 mM NaCl, respectively. Fitted curves were obtained using the two-site kinetic retention model. In (a) the relative effluent concentration is plotted as a function of pore volume. In (b) the normalized concentration (quality of the nHAP recovered in the sand, N_t, is divided by the quality in a unit volume of the input nHAP suspension, N_0) per gram of dry sand is plotted as a function of the distance from the column inlet.

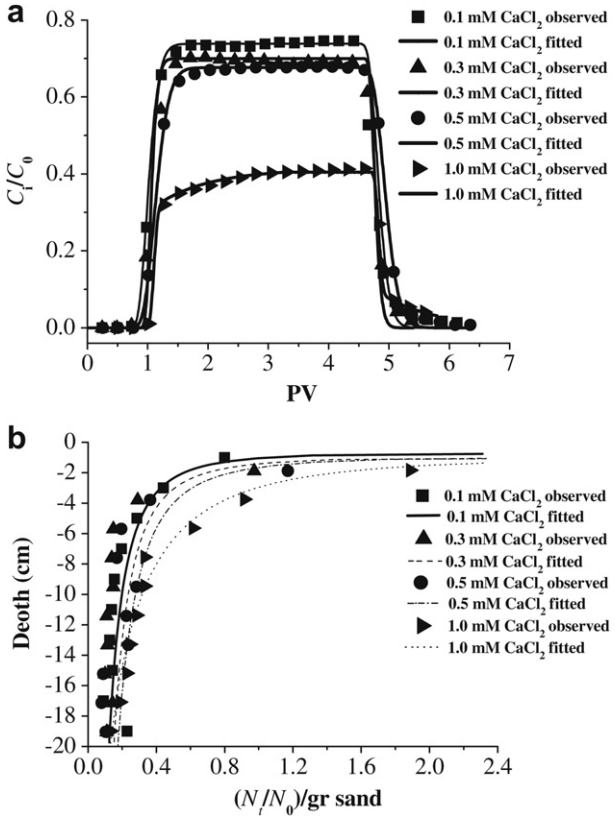

Fig. 2 – Measured and fitted breakthrough curves (a) and retention profiles (b) for nHAP under the IC of 0.1, 0.3, 0.5 and 1.0 mM $CaCl_2$, respectively. Fitted curves were obtained using the two-site kinetic retention. In (a) the relative effluent concentration is plotted as a function of pore volume. In (b) the normalized concentration (quality of the nHAP recovered in the sand, N_t, is divided by the quality in a unit volume of the input nHAP suspension, N_0) per gram of dry sand is plotted as a function of the distance from the column inlet.

Table 3 – Mass balance percentages for nHAP and Cu in the saturated packed column experiments at varying ISs and ICs used in this study.

NaCl (mM)	$CaCl_2$ (mM)	nHAP			Cu			
		Effluent[a]	Retained[b]	Total[c]	Effluent		Retained[f]	Total[g]
					nHAP-F[d]	Dis[e]		
		%						
0		89	7	96	39	39	15	93
1.0		80	15	95	33	38	20	91
10		68	28	96	15	38	36	89
50		44	50	94	12	38	44	94
100		11	79	90	8	38	47	93
	0.10	74	20	94	21	37	29	87
	0.30	68	27	95	17	39	36	92
	0.50	64	32	96	10	43	42	95
	1.0	26	65	91	3	46	45	94

a refers to the effluent percentage of nHAP recovered from column experiments.
b refers to the retained percentage of nHAP recovered from column experiments.
c refers to the total percentage of nHAP recovered from column experiments.
d refers to the percentage of nHAP-facilitated (nHAP-F) Cu in the effluent.
e refers to the percentage of dissolved Cu recovered in the effluent.
f refers to the retained percentage of Cu recovered from column experiments.
g refers to the total percentage of Cu recovered from column experiments.

confidence in our experimental procedures. Each co-transport experiment was duplicated and the replicated experiments exhibited similar transport and retention behavior for given conditions (data not shown).

Significant nHAP retention occurred despite the unfavorable electrochemical conditions for attachments in the primary minimum predicted by DLVO theory (Table 2). In general, an increase in the IS of the bulk solution resulted in increasing retention of the Cu-bearing nHAP onto the quartz grains for both monovalent and divalent cations. In particular, the percentage of nHAP mass that was recovered in the effluent decreased from 89 to 11% when the IS was increased from 0 to 100 mM of NaCl, and from 74 to 26% as the electrolyte concentration was raised from 0.1 to 1.0 mM of $CaCl_2$, respectively. Greater retention of Cu-bearing nHAP at higher electrolyte concentration can be explained in part by a reduction in the thickness of the double layer and a corresponding increase in the depth of the secondary minimum (Table 2). This finding is in accordance with previously reported literature (Elimelech et al., 1995; Walshe et al., 2010; Wang et al., 2011).

The retention profiles of Cu-bearing nHAP typically exhibited a hyperexponential shape with greater retention in the section adjacent to the column inlet (0–4 cm) and rapidly decreasing retention with depth (Figs. 1 and 2b). The shape of the retention profiles was not consistent with classical filtration theory (Yao et al., 1971) which predicts an exponential shape with depth. Hyperexponential profiles were more pronounced at higher electrolyte concentrations. For example, at IS = 0 about 40% of the total retained Cu-bearing nHAP were near the column inlet (<4 cm), whereas the value was as high as 65% at an IS of 100 mM NaCl (the same trend was observed for the Ca^{2+}). A number of potential explanations for hyperexponential retention profiles have been proposed in the literature including: chemical heterogeneity of colloids (Li et al., 2004; Tufenkji and Elimelech, 2005; Johnson and Li, 2005), straining of colloids (Bradford et al., 2002, 2003), secondary minimum and surface charge heterogeneity on the sand grain (Redman et al., 2004; Tufenkji and Elimelech, 2005; Johnson et al., 2010), surface roughness (Shellenberger and Logan, 2002; Yoon et al., 2006), colloid aggregation (Chen and Elimelech, 2006, 2007), and enhanced colloid retention in low velocity regions (Torkzaban et al., 2007, 2008; Bradford et al., 2009). These potential explanations will be discussed in greater detail in Section 3.4.

Figs. 1 and 2 present the simulated nHAP breakthrough curves and retention profiles for the various IS and IC conditions. Values of optimized model parameters are summarized in Table 4. The two-site kinetic retention model provides a good description of both the breakthrough curves and the retention profiles (see R^2 in Table 4). Values of k_1 and k_2 both increased with the electrolyte concentration of NaCl and $CaCl_2$, suggesting that the greater retention of nHAP was related to the depth of the secondary minimum (Tufenkji and Elimelech, 2005; Bradford et al., 2009). The percentage of retained nHAP in sites 1 and 2 were relatively constant with IS and IC, ranging from 30 to 37% on site 1 and 63–70% on site 2. The value of k_{1d} also increased with electrolyte concentration and was greater than or of a similar magnitude as k_1. Similar results have been observed elsewhere (Gargiulo et al., 2007, 2008).

3.3. *Effects of IS and IC on nHAP-F Cu transport*

The total and dissolved Cu concentrations of suspensions were measured before conducting the co-transport experiments. Table 2 indicates that the suspension pH and total Cu concentration varied from 5.7 to 5.9 and from 6.56 to 6.65 mg L^{-1}, respectively. The dissolved Cu concentration was little changed (2.42–2.46 mg L^{-1}) with IS when NaCl was the background electrolyte. However, the dissolved Cu

Table 4 – Fitted parameters of the two-kinetic attachment model as estimated from the breakthrough data for saturated packed quartz sand at varying ISs and ICs used in transport tests.[a]

Para[b]	NaCl (mM)					$CaCl_2$ (mM)			
	0	1	10	50	100	0.1	0.3	0.5	1.0
k_1 (min^{-1})	6.92e-03 (1.34e-03)	9.05e-03 (1.79e-03)	9.85e-03 (3.32e-03)	1.60e-02 (6.52e-03)	5.57e-02 (2.81e-01)	7.40e-03 (1.65e-03)	8.21e-03 (5.70e-03)	1.04e-02 (5.67e-03)	4.87e-02 (6.57e-02)
k_{1d} (min^{-1})	2.98e-02 (6.17e-03)	3.88e-02 (8.06e-03)	4.15e-02 (1.44e-02)	4.05e-02 (2.23e-02)	2.42e-01 (1.32e+00)	3.68e-02 (8.82e-03)	4.14e-02 (2.99e-02)	4.47e-02 (2.53e-02)	3.47e-01 (5.32e-01)
k_2 (min^{-1})	4.82e-02 (1.78e-03)	5.52e-02 (1.90e-03)	7.87e-02 (2.99e-03)	1.52e-01 (7.78e-03)	4.91e-01 (3.27e-02)	7.60e-02 (2.12e-03)	8.7e-02 (5.07e-03)	9.70e-02 (4.93e-03)	2.55e-01 (9.90e-03)
Mass site 1 (%)	2.4	5.6	9.9	17.7	24.1	6.4	8.5	10.9	19.8
Mass site 2 (%)	4.6	9.4	18.1	32.3	54.9	13.6	18.5	21.1	45.2
β	0.432	0.432	0.432	0.432	0.432	0.432	0.432	0.432	0.432
R^2	0.994	0.991	0.979	0.911	0.942	0.990	0.949	0.951	0.951

a 95% confident intervals on fitted parameters are shown in parentheses.
b Parameters: k_1, the first-order retention coefficient on site 1; k_{1d}, the first-order detachment coefficient on site 1; k_2, the first-order detachment coefficient on site 2; Mass sites 1 and 2 are percentages of mass of Cu-bearing nHAP deposited on site 1 and 2, respectively; β, empirical factor controlling the shape of the spatial distribution; R^2, Person's squared correlation coefficient.

concentration changed from 2.38 to 2.96 mg L^{-1} when the electrolyte concentration was increased from 0.1 to 1.0 mM of $CaCl_2$. This observation suggests that the divalent Ca^{2+} competes with Cu^{2+} for ion-exchange sites on nHAP. Even through the ion selectivity coefficients favor the adsorption of Cu^{2+} over Ca^{2+} (Bakker, 1997), the larger concentration (4–40 mg L^{-1}) of Ca^{2+} displaces some of the Cu^{2+} on nHAP exchange sites.

Fig. 3 shows representative breakthrough curves for nHAP-F Cu under the various IS and IC conditions. Corresponding mass balance information for the dissolved and nHAP-F Cu in the column effluents is provided in Table 3. The solution chemistry had a marked effect on the co-transport of Cu with nHAP. Increasing the IS of the solution reduced the peak effluent concentration and total mass of nHAP-F Cu. The peak effluent concentrations of nHAP-F Cu diminished from 2.62 to 0.17 mg L^{-1} as the concentration of NaCl increased from 0 to 100 mM (Fig. 3a) and from 1.58 to 0.16 mg L^{-1} as the concentration of $CaCl_2$ increased from 0.1 to 1.0 mM (Fig. 3b). The nHAP-F Cu accounted for about 39 and 8% of the total Cu in the effluent at an IS of 0 and 100 mM, respectively. Similarly, nHAP-F Cu decreased from 21 to 3% of the total Cu in the effluent when the concentration of $CaCl_2$ increased from 0.1 to 1.0 mM (Table 3). Qualitatively similar relationships of colloid-facilitated contaminant transport with IS and IC have been reported elsewhere (Cheng and Saiers, 2010; Walshe et al., 2010). The decline in Cu transport with increasing IS reflects the influences of IS on Cu-bearing nHAP mobility discussed in the previous section and on the partitioning of Cu between nHAP and dissolved phases. As mentioned above, divalent Ca^{2+} competes with Cu^{2+} for ion-exchange sites on nHAP and this leads to enhanced dissociation of Cu into bulk solution, whereas dissolved Cu was relatively unaffected with increasing concentration of NaCl (Table 3). Thus, decreases in the suspended load (increased retention of Cu-bearing nHAP) combined with decreases in the affinity of Cu for nHAP (increased ion exchange) accounted for the observed decline in nHAP-F Cu mobilization with increasing IS. It should be noted that dissolved Cu actually accounted for a greater percentage of the total Cu in the effluent than nHAP-F Cu, especially as the concentration of NaCl and $CaCl_2$ increased in solution (Table 3). This observation indicates that nHAP tended to inhibit Cu transport because of retention of nHAP-F Cu.

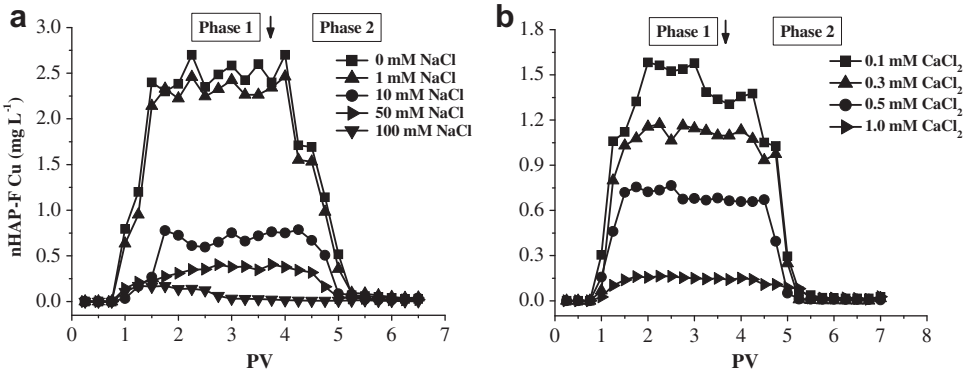

Fig. 3 – Representative breakthrough curves for nHAP-F Cu as a function of PV under different concentrations of NaCl (a) and $CaCl_2$ (b) of bulk solution, respectively. Note that the concentration of nHAP-F Cu was calculated as the difference between dissolved and total Cu of Cu-bearing nHAP suspension.

3.4. *Mechanisms influencing nHAP retention and nHAP-F Cu transport*

The above information clearly indicates that factors that influence the retention of nHAP will have a large impact on the facilitated transport of Cu. Additional experiments were therefore conducted to better understand and quantify the mechanisms of nHAP retention.

The nHAP transport experiments shown in Figs. 1 and 2 indicate that increasing retention occurred with increasing NaCl and $CaCl_2$ concentrations. Under chemically unfavorable attachment conditions (electrostatic repulsion), nHAP may interact with the solid phase by virtue of the presence of the reversible secondary minimum at a small separation distance (Franchi and O'Melia, 2003; Redman et al., 2004; Tufenkji and Elimelech, 2005). In order to further test this hypothesis, we ran several three phase transport experiments using 200 mg L^{-1} of nHAP and 0.1 mM of Cu. Phases 1 and 2 were the same as for other experiments described above, whereas phase 3 consisted of flushing the column with several pore volumes of ultrapure water (IS = 0) to eliminate the secondary minimum (Franchi and O'Melia, 2003). Release of previously deposited colloids through lowering the bulk solution IS has been used as supportive evidence for particle deposition in the secondary minimum (Franchi and O'Melia, 2003; Redman et al., 2004; Tufenkji and Elimelech, 2005).

The breakthrough curves for the three phase experiments at the electrolyte concentrations of 100 mM of NaCl and 1.0 mM of $CaCl_2$ are shown in Fig. 4a and b, respectively. The transport and retention of nHAP during phases 1 and 2 was similar to that previously discussed for Figs. 1 and 2 (Table 3). In Fig. 4a (100 mM NaCl during phases 1 and 2) rinsing the column with ultrapure water during phase 3 resulted in a sharp peak ($C_i/C_0 = 1.7$) of released nHAP that accounted for approximately 35% of the previously retained mass. In contrast, in Fig. 4b (1.0 mM $CaCl_2$ during phases 1 and 2) rinsing the column with ultrapure water during phase 3 resulted in a minor peak ($C_i/C_0 = 0.04$) and release of retained nHAP in the effluent. These observations suggest that the secondary minimum was likely involved in the nHAP retention for both 100 mM NaCl and 1.0 mM $CaCl_2$ systems, but that it cannot account for most of the retained nHAP mass.

The ζ-potential of nHAP suspensions at IS = 0 was measured before and after filtering them through a 1 μm pore diameter glass fiber filter in order to test the hypothesis of nHAP surface charge heterogeneity. The value of the nHAP ζ-potential increased from −53.0 to −60.4 mV before and after filtering at IS = 0. Li et al. (2004) reported that such a variation in the ζ-potential was sufficient to cause hyperexponential retention profiles. Specifically, the fraction of the colloid population with higher (less negative) ζ-potentials is assumed to preferentially attach at the column inlet, whereas the remaining particles experience a slower attachment rate and greater transport potential.

Straining of colloids at grain–grain contacts has been considered to be insignificant when the diameter ratio of colloid to grain is less than 0.005 (Bradford et al., 2003; Johnson et al., 2007). In this study, the diameter ratio of Cu-bearing nHAP aggregates to sand was more than an order of magnitude lower than this threshold. Straining of nHAP aggregates at grain–grain contacts was therefore not considered to be important.

Surface roughness has been demonstrated to play a critical role in colloid deposition (Shellenberger and Logan, 2002; Yoon et al., 2006; Torkzaban et al., 2010). Similar to grain–grain contacts, surface roughness locations are low velocity regions that are associated with lower hydrodynamic forces and torques and flow vortices (Vaidyanathan and Tien, 1988; Taneda, 1979), and therefore enhanced colloid retention under unfavorable attachment conditions. In particular, when the colloid radius is less than the roughness height, the applied hydrodynamic torque will be zero and create locations that are hydrodynamic favorable for colloid deposition even for an IS of zero (Vaidyanathan and Tien, 1988). In addition, Torkzaban et al. (2010) demonstrated that nanoscale surface roughness can create locally favorable conditions for nanoscale colloid deposition.

Fig. 5a shows a SEM image of a cleaned quartz sand grain. This grain possesses significant surface roughness of different sizes, ranging from several nanometers to dozens of microns. Considering that the length of nHAP is 100 nm, these rough patches can likely create local regions that are hydrodynamically favorable for nHAP retention. Fig. 5b shows an SEM image of quartz sand excavated from the column inlet after

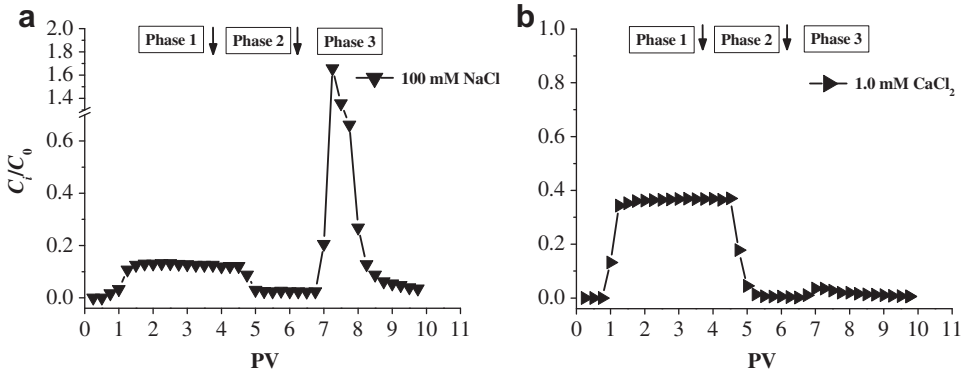

Fig. 4 – The three phase breakthrough curves for Cu-bearing nHAP under electrolyte concentration of (a) 100 mM of NaCl, and (b) 1.0 mM of $CaCl_2$, respectively. Phase 1: Cu-bearing nHAP suspension, phase 2: eluted with background electrolyte solution, and phase 3: further eluted with ultrapure water.

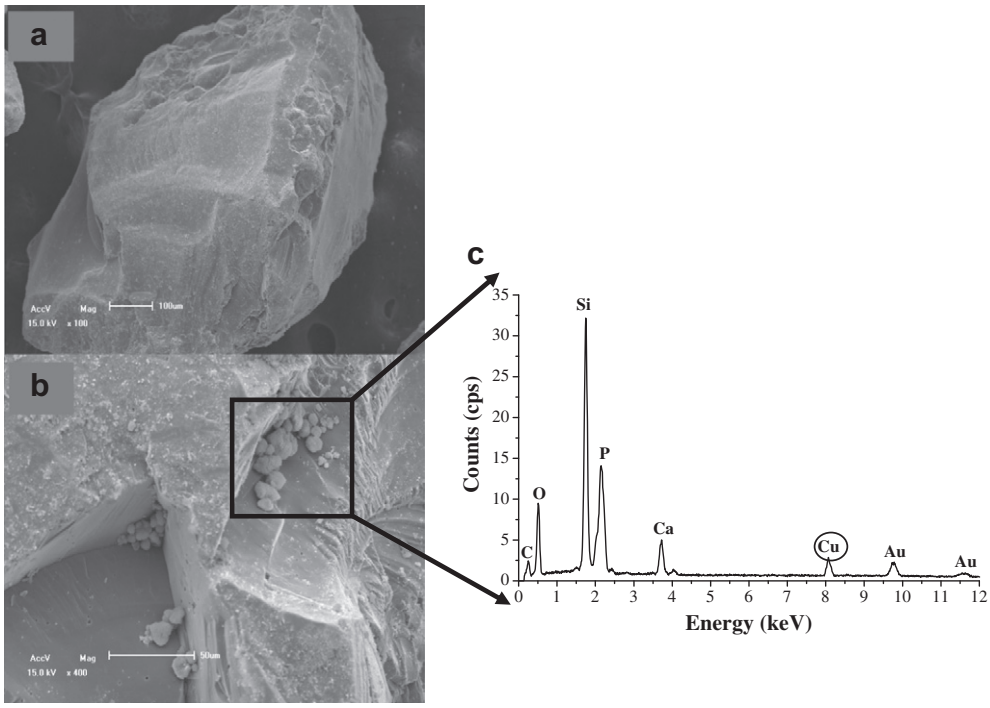

Fig. 5 – SEM micrographs of cleaned quartz sand (a) and the quartz sand excavated from the inlet of the packed column (b) after completion of the Cu-bearing nHAP transport test using 1.0 mM of $CaCl_2$. On the right (c) is the corresponding EDX spectrum of the retained nHAP on the quartz sand marked in the box.

completion of the transport test at bulk solution IS of 1.0 mM of $CaCl_2$. Fig. 5b demonstrates that large spherical-like aggregates were retained at surface roughness locations. Furthermore, the aggregates were not uniformly distributed on the grain surface as would be expected for secondary and/or primary minimum attachment upon collision with the sand, even though a large secondary minimum of −4.4 occurred for this system. The result of an EDX chemical analysis of these aggregates is presented in Fig. 5c. The presence of Ca, P and O elements are consistent with the basic components of nHAP, and the Cu peak confirms that the large aggregates were composed of Cu-bearing nHAP. Neither Fe nor Al oxides were present on the surfaces of the quartz grain, suggesting low amounts of chemical heterogeneity.

To further test the hypothesis that nHAP aggregation influenced transport and retention, the hydrodynamic diameter distribution of nHAP in the effluent was determined by DLS measurement after completion of the co-transport experiment using 1.0 mM of $CaCl_2$. The hydrodynamic diameter distribution ranged from 150 to 250 nm, with a mean diameter of 210 ± 5 nm. This size distribution is much larger than that for the influent suspension of nHAP in 1.0 mM of NaCl solution (135 ± 5 nm). The nHAP tended to form larger aggregates in the presence of divalent Ca^{2+} than monovalent Na^{+} likely because Ca^{2+} acted as a bridging agent (Wang et al., 2011).

The above information indicates that the secondary minimum, nHAP surface charge heterogeneity, surface roughness, and aggregation are involved in the retention of nHAP. An explanation of the interrelation of these factors on nHAP retention is briefly discussed below. The probability that colloids colliding with the grain will remain associated with the solid has been estimated from the depth of the secondary minimum (which is a function of IS and IC in Table 2) under unfavorable attachment conditions (Ryan and Elimelech, 1996; Simoni et al., 1998; Shen et al., 2007). However, this approach neglects the effects of hydrodynamics and pore space geometry on colloid retention as revealed by Torkzaban et al. (2008). Colloids that are weakly associated with the solid surface via the secondary minimum can be translated and/or funneled by fluid drag forces to such low velocity regions and "eddy zones" at locations associated with surface roughness or grain–grain contact points where they are immobilized (Kuznar and Elimelech, 2007; Torkzaban et al., 2008, 2010). A larger number of colloids may enter these low velocity regions at higher electrolyte concentrations due to the greater depth of the secondary minimum. In addition, aggregated nHAP experience a greater depth of the secondary minimum and hydrodynamic forces than smaller colloids (e.g., Bradford et al., 2011). Hence, the amount of nHAP retention (see k_1 and k_2 in Table 4) is expected to be greater with increasing electrolyte concentration and nHAP size (aggregation). Hyperexponential profiles will be influenced by nHAP surface charge heterogeneity (Li et al., 2004; Tufenkji and Elimelech, 2005) as well as the hydrodynamics to low velocity regions (Bradford et al., 2009) such as surface roughness locations.

4. Conclusions

Facilitated transport of Cu by nHAP in water-saturated quartz sand was found to be a strong function of the solution IS and

IC. In particular, the concentration of nHAP-F Cu declined significantly from 2.62 to 0.17 mg L^{-1} when NaCl increased from 0 to 100 mM, and from 1.58 to 0.16 mg L^{-1} when $CaCl_2$ increased from 0.1 to 1.0 mM. The total mass recovery of Cu in the effluent solution exhibited the same trend. This facilitated transport behavior was due to difference in the capacity of nHAP to bind Cu and the retention of nHAP with changes in IS and IC. The capacity of nHAP to bind Cu^{2+} decreased with increasing concentrations of Ca^{2+} as a result of ion exchange. More importantly, the amount of Cu-bearing nHAP that was retained in the sand increased with solution concentration of NaCl and especially $CaCl_2$. Most of the Cu-bearing nHAP was retained close to the column inlet (0–4 cm), and the rate of retention rapidly decreased with depth. The experimental breakthrough curves and retention profiles of nHAP were well described using a mathematical model based on the CDE and two kinetic retention sites. Site 1 considered reversible retention, whereas site 2 was for irreversible, depth-dependent retention. The first-order retention coefficients on both site 1 (k_1) and 2 (k_2) increased with the NaCl and $CaCl_2$ concentration due to increases in the depth of the secondary minimum. However, elimination of the secondary minimum after recovery of the breakthrough curves did not release the majority of the retained nHAP. SEM images in association with EDX measurements and DLS information demonstrated that nHAP aggregated occurred and that retention was strongly influenced by the grain surface roughness.

Acknowledgments

The authors grateful acknowledge the support of the National Basic Research and Development Program (2007CB936604), the Knowledge Innovative project of Chinese Academy of Sciences (KZCX2-YW-Q02-02) and the open fund of the State Key Laboratory of Soil and Sustainable Agriculture (Y052010027). M. Paradelo is granted by the FPU program from the Spanish Ministry of Education. We are grateful to the critical review of Dr. J. Eugenio Lopez (University of Vigo) that led to revision and substantial improvement of this manuscript.

REFERENCES

Bakker, E., 1997. Determination of unbiased selectivity coefficients of neutral-carrier based cation-selective electrodes. Analytical Chemistry 69 (6), 1061–1069.

Boussiba, S., Richmond, A.E., 1979. Isolation and characterization of phycocyanins from the blue-green alga *Spirulina platensis*. Archives of Microbiology 120 (2), 155–159.

Bradford, S.A., Kim, H., 2010. Implications of cation exchange on clay release and colloid-facilitated transport in porous media. Journal of Environmental Quality 39 (6), 2040–2046.

Bradford, S.A., Yates, S.R., Bettahar, M., Simunek, J., 2002. Physical factors affecting the transport and fate of colloids in saturated porous media. Water Resource Research 38. doi:10.1029/2002WR001340.

Bradford, S.A., Simunek, J., Bettahar, M., van Genuchten, M.T., Yates, S.R., 2003. Modeling colloid attachment, straining, and exclusion in saturated porous media. Environmental Science & Technology 37 (10), 2242–2250.

Bradford, S.A., Torkzaban, S., Leij, F., Simunek, J., van Genuchten, M.T., 2009. Modeling the coupled effects of pore space geometry and velocity on colloid transport and retention. Water Resources Research 45. doi:10.1029/2008WR007096.

Bradford, S.A., Torkzaban, S., Wiegmann, A., 2011. Pore-scale simulations to determine the applied hydrodynamic torque and colloid immobilization. Vadose Zone Journal 10 (1), 252–261.

Chen, K.L., Elimelech, M., 2006. Aggregation and deposition kinetics of fullerene (C-60) nanoparticles. Langmuir 22 (26), 10994–11001.

Chen, K.L., Elimelech, M., 2007. Influence of humic acid on the aggregation kinetics of fullerene (C-60) nanoparticles in monovalent and divalent electrolyte solutions. Journal of Colloid and Interface Science 309 (1), 126–134.

Cheng, T., Saiers, J.E., 2010. Colloid-facilitated transport of cesium in vadose-zone sediments: the importance of flow transients. Environmental Science & Technology 44 (19), 7443–7449.

de Jonge, L.W., Kjaergaard, C., Moldrup, P., 2004. Colloids and colloid-facilitated transport of contaminants in soils: an introduction. Vadose Zone Journal 3 (2), 321–325.

Derjaguin, B., Landau, L., 1941. Theory of the stability of strongly charged lyophobic sols and of the adhesion of strongly charged particles in solutions of electrolytes. Acta Physicochima USSR 14, 633–662.

Elimelech, M., Gregory, J., Jia, X., Williams, R.A., 1995. Particle Deposition and Aggregation: Measurement, Modeling and Simulation. Butterworth-Heinemann Ltd., Oxford.

Fang, J., Shan, X.Q., Wen, B., Lin, J.M., Owens, G., Zhou, S.R., 2011. Transport of copper as affected by titania nanoparticles in soil columns. Environmental Pollution 159 (5), 1248–1256.

Franchi, A., O'Melia, C.R., 2003. Effects of natural organic matter and solution chemistry on the deposition and reentrainment of colloids in porous media. Environmental Science & Technology 37 (6), 1122–1129.

Gargiulo, G., Bradford, S.A., Simunek, J., Ustohal, P., Vereecken, H., Klumpp, E., 2007. Transport and deposition of metabolically active and stationary phase *Deinococcus radiodurans* in unsaturated porous media. Environmental Science & Technology 41 (4), 1265–1271.

Gargiulo, G., Bradford, S.A., Simunek, J., Ustohal, P., Vereecken, H., Klumpp, E., 2008. Bacteria transport and deposition under unsaturated flow conditions: the role of water content and bacteria surface hydrophobicity. Vadose Zone Journal 7 (2), 406–419.

Grolimund, D., Borkovec, M., Barmettler, K., Sticher, H., 1996. Colloid-facilitated transport of strongly sorbing contaminants in natural porous media: a laboratory column study. Environmental Science & Technology 30 (10), 3118–3123.

Handley-Sidhu, S., Renshaw, J.C., Moriyama, S., Stolpe, B., Mennan, C., Bagheriasl, S., Yong, P., Stamboulis, A., Paterson-Beedle, M., Sasaki, K., Pattrick, R.A.D., Lead, J.R., Macaskie, L.E., 2011. Uptake of Sr^{2+} and Co^{2+} into biogenic hydroxyapatite: implications for biomineral ion exchange synthesis. Environmental Science & Technology 45 (16), 6985–6990.

Israelachvili, J.N., 1992. Intermolecular and Surface Forces. Academic, New York.

Johnson, W.P., Li, X.Q., 2005. Comment on breakdown of colloid filtration theory: role of the secondary energy minimum and surface charge heterogeneities. Langmuir 21 (23), 10895.

Johnson, W.P., Li, X.Q., Assemi, S., 2007. Deposition and re-entrainment dynamics of microbes and non-biological colloids during non-perturbed transport in porous media in the presence of an energy barrier to deposition. Advances in Water Resources 30 (6–7), 1432–1454.

Johnson, W.P., Pazmino, E., Ma, H.L., 2010. Direct observations of colloid retention in granular media in the presence of energy barriers, and implications for inferred mechanisms from indirect observations. Water Research 44 (4), 1158–1169.

Kim, H.N., Walker, S.L., Bradford, S.A., 2010. Coupled factors influencing the transport and retention of *Cryptosporidium parvum* oocysts in saturated porous media. Water Research 44 (4), 1213–1223.

Kuznar, Z.A., Elimelech, M., 2007. Direct microscopic observation of particle deposition in porous media: role of the secondary energy minimum. Colloids and Surfaces A: Physicochemical and Engineering Aspects 294 (1–3), 156–162.

Li, X.Q., Scheibe, T.D., Johnson, W.P., 2004. Apparent decreases in colloid deposition rate coefficients with distance of transport under unfavorable deposition conditions: a general phenomenon. Environmental Science & Technology 38 (21), 5616–5625.

Ma, Q.Y., Traina, S.J., Logan, T.J., Ryan, J.A., 1994. Effects of aqueous Al, Cd, Cu, Fe(II), Ni, and Zn on Pb immobilization by hydroxyapatite. Environmental Science & Technology 28 (7), 1219–1228.

Marquardt, D.W., 1963. An algorithm for least-squares estimation of nonlinear parameters. Journal of the Society for Industrial and Applied Mathematics 11 (2), 431–441.

McCarthy, J.F., Zachara, J.M., 1989. Subsurface transport of contaminants. Environmental Science & Technology 23 (5), 496–502.

Onuma, K., Oyane, A., Tsutsui, K., Tanaka, K., Treboux, G., Kanzaki, N., Ito, A., 2000. Precipitation kinetics of hydroxyapatite revealed by the continuous-angle laser light-scattering technique. The Journal of Physical Chemistry B 104 (45), 10563–10568.

Redman, J.A., Walker, S.L., Elimelech, M., 2004. Bacterial adhesion and transport in porous media: role of the secondary energy minimum. Environmental Science & Technology 38 (6), 1777–1785.

Roy, S.B., Dzombak, D.A., 1997. Chemical factors influencing colloid-facilitated transport of contaminants in porous media. Environmental Science & Technology 31 (3), 656–664.

Ryan, J.N., Elimelech, M., 1996. Colloid mobilization and transport in groundwater. Colloids and Surfaces A: Physicochemical and Engineering Aspects 107, 1–56.

Schijven, J.F., Simunek, J., 2002. Kinetic modeling of virus transport at the field scale. Journal of Contaminant Hydrology 55 (1–2), 113–135.

Shellenberger, K., Logan, B.E., 2002. Effect of molecular scale roughness of glass beads on colloidal and bacterial deposition. Environmental Science & Technology 36 (2), 184–189.

Shen, C.Y., Li, B.G., Huang, Y.F., Jin, Y., 2007. Kinetics of coupled primary- and secondary-minimum deposition of colloids under unfavorable chemical conditions. Environmental Science & Technology 41 (20), 6976–6982.

Simoni, S.F., Harms, H., Bosma, T.N.P., Zehnder, A.J.B., 1998. Population heterogeneity affects transport of bacteria through sand columns at low flow rates. Environmental Science & Technology 32 (14), 2100–2105.

Simunek, J., He, C.M., Pang, L.P., Bradford, S.A., 2006. Colloid-facilitated solute transport in variably saturated porous media: numerical model and experimental verification. Vadose Zone Journal 5 (3), 1035–1047.

Simunek, J., Sejna, M., van Genuchten, M.T., 2008. The HYDRUS-1D Software Package for Simulating the One-dimensional Movement of Water, Heat, and Multiple Solutes in Variably-saturated Media. Version 4. Beta 1. ICGWMC-TPS-70. International Ground Water Modeling Center, Colorado School of Mines, Golden, Colorado.

Smiciklas, I., Dimovic, S., Plecas, I., Mitric, M., 2006. Removal of Co^{2+} from aqueous solutions by hydroxyapatite. Water Research 40 (12), 2267–2274.

Stankovich, S., Piner, R.D., Nguyen, S.T., Ruoff, R.S., 2006. Synthesis and exfoliation of isocyanate-treated graphene oxide nanoplatelets. Carbon 44 (15), 3342–3347.

Taneda, S., 1979. Visualization of separating Stokes flows. Journal of the Physical Society of Japan 46 (6), 1935–1942.

Torkzaban, S., Bradford, S.A., Walker, S.L., 2007. Resolving the coupled effects of hydrodynamics and DLVO forces on colloid attachment in porous media. Langmuir 23 (19), 9652–9660.

Torkzaban, S., Tazehkand, S.S., Walker, S.L., Bradford, S.A., 2008. Transport and fate of bacteria in porous media: coupled effects of chemical conditions and pore space geometry. Water Resources Research 44 (4). doi:10.1029/2007WR006541.

Torkzaban, S., Kim, H.N., Simunek, J., Bradford, S.A., 2010. Hysteresis of colloid retention and release in saturated porous media during transients in solution chemistry. Environmental Science & Technology 44 (5), 1662–1669.

Tufenkji, N., Elimelech, M., 2005. Breakdown of colloid filtration theory: role of the secondary energy minimum and surface charge heterogeneities. Langmuir 21 (3), 841–852.

Vaidyanathan, R., Tien, C., 1988. Hydrosol deposition in granular beds. Chemical Engineering Science 43 (2), 289–302.

Verwey, E.J.M., Overbeek, J.T.G., 1948. Theory of the Stability of Lyophobic Colloids. Elsevier, Amsterdam.

Walshe, G.E., Pang, L.P., Flury, M., Close, M.E., Flintoft, M., 2010. Effects of pH, ionic strength, dissolved organic matter, and flow rate on the co-transport of MS2 bacteriophages with kaolinite in gravel aquifer media. Water Research 44 (4), 1255–1269.

Wang, D.J., Chu, L.Y., Paradelo, M., Peijnenburg, J.M.G.W., Wang, Y.J., Zhou, D.M., 2011. Transport behavior of humic acid-mediated nano-hydroxyapatite in saturated packed column: effects of Cu, ionic strength, and ionic composition. Journal of Colloid and Interface Science 360 (2), 398–407.

Yao, K.M., Habibian, M.T., O'melia, C.R., 1971. Water and waste water filtration: concepts and applications. Environmental Science & Technology 5 (11), 1105–1112.

Yoon, J.S., Germaine, J.T., Culligan, P.J., 2006. Visualization of particle behavior within a porous medium: mechanisms for particle filtration and retardation during downward transport. Water Resources Research 42 (6). doi:10.1029/2004WR003660.

Zhang, L.L., Wang, L.L., Zhang, P., Kan, A.T., Chen, W., Tomson, M.B., 2011. Facilitated transport of 2, 2′, 5, 5′-polychlorinated biphenyl and phenanthrene by fullerene nanoparticles through sandy soil columns. Environmental Science & Technology 45 (4), 1341–1348.

Zhou, D.M., Wang, D.J., Cang, L., Hao, X.Z., Chu, L.Y., 2011. Transport and re-entrainment of soil colloids in saturated packed column: effects of pH and ionic strength. Journal of Soils and Sediments 11 (3), 491–503.